Journal of Geophysical Research: Space Physics

RESEARCH ARTICLE
10.1029/2017JA025164

Seasonal Variability of the Midlatitude Traveling Ionospheric Disturbances From Wallops Island, VA, Dynasonde Data: Evidence of a Semiannual Variation

Catalin Negrea[1], Nikolay Zabotin[2], and Terence Bullett[3,4]

[1]Institute of Space Science, Măgurele, Romania, [2]Department of Electrical and Computer Engineering, University of Colorado Boulder, Boulder, CO, USA, [3]Cooperative Institute for Research in Environmental Sciences, University of Colorado Boulder, Boulder, CO, USA, [4]NOAA NCEI, Boulder, CO, USA

Key Points:
- The seasonal variability due to TIDs in the bottomside *F* layer is investigated using Dynasonde data obtained at Wallops Island, VA
- A semiannual variation is observed in the overall level of TID activity using the Doppler speed PSD
- A semiannual variation is observed in the dominant propagation direction of TIDs using the zonal and meridional tilt PSD

Correspondence to:
C. Negrea,
negreacatalin@gmail.com

Citation:
Negrea, C., Zabotin, N., & Bullett, T. (2018). Seasonal variability of the midlatitude traveling ionospheric disturbances from Wallops Island, VA, Dynasonde data: Evidence of a semiannual variation. *Journal of Geophysical Research: Space Physics*, *123*, 5047–5054. https://doi.org/10.1029/2017JA025164

Received 11 JAN 2018
Accepted 17 MAY 2018
Accepted article online 22 MAY 2018
Published online 5 JUN 2018

Abstract We investigate the ionospheric variability due to traveling ionospheric disturbances (TIDs) over Wallops Island, VA, using Dynasonde-derived measurements of ionospheric tilts and vertical Doppler speed between May 2013 and August 2016, covering the bottomside ionospheric *F* layer. The mean power spectral density is determined separately for each month for both ionospheric tilts and for the Doppler speed, with a 2 km resolution in a broad altitude range. This is accomplished using a spectral analysis technique based on the Lomb-Scargle and Welch methods, with an added filtering criterion. The analysis is performed separately for the daytime and nighttime data. By investigating the seasonal variability of the power spectral density integral, a semiannual variation is highlighted in the overall level of daytime TID activity, with increased activity during summer and winter seasons in the northern hemisphere. This result provides a more complete picture than other recent publications that only highlighted a winter peak in the same geographical sector. Finally, the relative amplitude of the two peaks in TID activity is shown to vary significantly during the three years investigated and also as a function of the altitude.

1. Introduction

Traveling ionospheric disturbances (TIDs) are wave-like oscillations of the ionospheric plasma. These are often caused by underlying acoustic-gravity waves (AGWs), which has allowed for a multitude of remote sensing studies to use TIDs as tracers for AGW activity using measurement from incoherent scatter radars (Djuth et al., 2010; Oliver et al., 1994), Super Dual Auroral Radar Network (SuperDARN; Bristow et al., 1994; Ishida et al., 2008), airglow all-sky imagers (Otsuka et al., 2004; Shiokawa et al., 2003), Global Positioning System total electron content (Borries et al., 2009; Otsuka et al., 2013), and Dynasondes (Negrea et al., 2016; Zabotin et al., 2016). A number of these studies have focused on the specifics of the seasonal variability of AGW and TID activity (Garcia et al., 2000; Grocott et al., 2013; Hernandez-Pajares et al., 2006; Kotake et al., 2006; Shiokawa et al., 2003). Because of the characteristics and limitations of individual measurement techniques, different TID populations can be highlighted depending on the investigation method used.

Recent work has highlighted the existence of an annual variation of the TID activity with a winter peak over the North American sector and a sharp decrease during summer (Frissell et al., 2014, 2016). A possible instrumentation bias discussed by Frissell et al. (2014) might influence these results. Generally, geographical coverage of existing instruments is limited, height stratified results cannot be obtained using most of the established techniques, and there are other fundamental limitations inherent to all of them. That is why long-term variability of TIDs and AGWs still requires more investigation. This paper aims to clarify the nature of the seasonal variability of midlatitude TIDs using Dynasonde measurements of ionospheric tilts and the vertical component of the Doppler speed, taken at Wallops Island, VA, from May 2013 to August 2016. The quality of Dynasonde data sets can be considered equivalent to that provided by incoherent scatter radars (Sedgemore et al., 1996), with the advantage that, in general, Dynasonde data sets cover a significantly larger time interval, and the disadvantage of a lack of coverage in two altitude ranges: the *E-F* "valley" and the topside *F* layer. We determine a mean power spectral density (PSD) for each month in the selected interval, between 140 and 320 km altitude with a 2 km resolution. The method has been described in detail by Negrea and Zabotin (2016), and it allows for an accurate determination of the mean PSD, regardless of the underlying data sampling. The PSD integral is then used as an estimator for the ionospheric variability. Unlike the previous studies conducted using other data sources, we are able to obtain height stratified

results due to the ability of Dynasonde-capable instruments to observe the bottomside ionosphere over an extended altitude range and due to high resolution of the inversion methods associated with the Dynasonde data analysis. Our results demonstrate the presence of both the previously reported annual variation and a semiannual variation.

Section 2 of this paper describes the basics of the Dynasonde techniques and of the analysis methodology. Section 3 presents and discusses the results, and section 4 contains our conclusions.

2. Dynasonde Data and Analysis Methodology

This study uses a 40-monthlong data set between May 2013 and August 2016, obtained using the vertical incidence pulsed ionospheric radar system at Wallops Island, VA, which operates at a cadence of 1–2 min. The specifics of the Dynasonde analysis have been discussed in recent publications by Negrea et al. (2016) and Zabotin et al. (2016), and further details can be found in Zabotin et al. (2006) Wright and Pitteway (1999), Wright and Pitteway (1979), and Paul et al. (1974). The exact same method is used in this study. Of particular importance is the plasma density inversion procedure NeXtYZ based on the wedge-stratified ionosphere model (Zabotin et al., 2006), which assumes a height-stratified ionosphere with each surface of constant plasma density being a portion of a tilted plane in the vicinity of the vertical axis. The ionospheric "tilts" (n_x, n_y) are rigorously defined as the horizontal components of the unit vector describing the direction of the total plasma density gradient:

$$\vec{n} = (n_x, n_y, n_z) = \frac{\vec{\nabla} N_e}{\left|\vec{\nabla} N_e\right|} \tag{1}$$

This is one of the products of the NeXtYZ inversion procedure, others being the vertical electron density profile with associated uncertainties and the vertical component of the Doppler speed. Note that both ionospheric tilts are dimensionless.

A TID harmonic is represented locally by a simple wave model:

$$N_e' = N_e'(z,\omega)\exp[i(\boldsymbol{k}\cdot\boldsymbol{r} - \omega t)] \tag{2}$$

$$v_z' = v_z'(z,\omega)\exp[i(\boldsymbol{k}\cdot\boldsymbol{r} - \omega t)] \tag{3}$$

where $N_e'(z,\omega)$ and $v_z'(z,\omega)$ are the magnitudes of that specific harmonic in electron density and Doppler speed, respectively, $\boldsymbol{k} = (k_x, k_y, k_z)$ and ω are its wave vector and angular frequency, $\boldsymbol{r} = (x, y, z)$ is the position vector, and t is the time. Both the electron density and the Doppler speed can therefore be used to extract the amplitude of a single TID harmonic. However, the measured electron density (N_e) is the sum of a background component ($\overline{N_e}$) and the perturbation term (N_e'):

$$N_e(\boldsymbol{r}, t) = \overline{N_e}(\boldsymbol{r}, t) + N_e'(\boldsymbol{r}, t) \tag{4}$$

where $\overline{N_e}$ is controlled primarily by solar UV radiation-induced ion production and loss, and by geomagnetic forcing, and is generally an order of magnitude higher than N_e'. Extraction of the perturbation part of the electron density variations requires detrending of the data, what may incur additional errors. The plasma drift does not contain a similarly dominant background component, that is why its use was preferred for this analysis.

In addition to the Doppler speed, the two ionospheric tilts are used. In addition to being proportional to the TID amplitude, they also allow distinguishing between waves propagating in the zonal and meridional directions. Equations (1) and (2) can be combined to show

$$n_{x,y} = \frac{k_{x,y}}{\left|\nabla \overline{N_e}\right|} N_e' \tag{5}$$

where $k_{x,y}$ are the zonal and meridional components of the wave vector, $\boldsymbol{k}$. Additionally, the normalization by $\left|\nabla \overline{N_e}\right|$ reduces the sensitivity of the tilts to altitude variations in the background electron density.

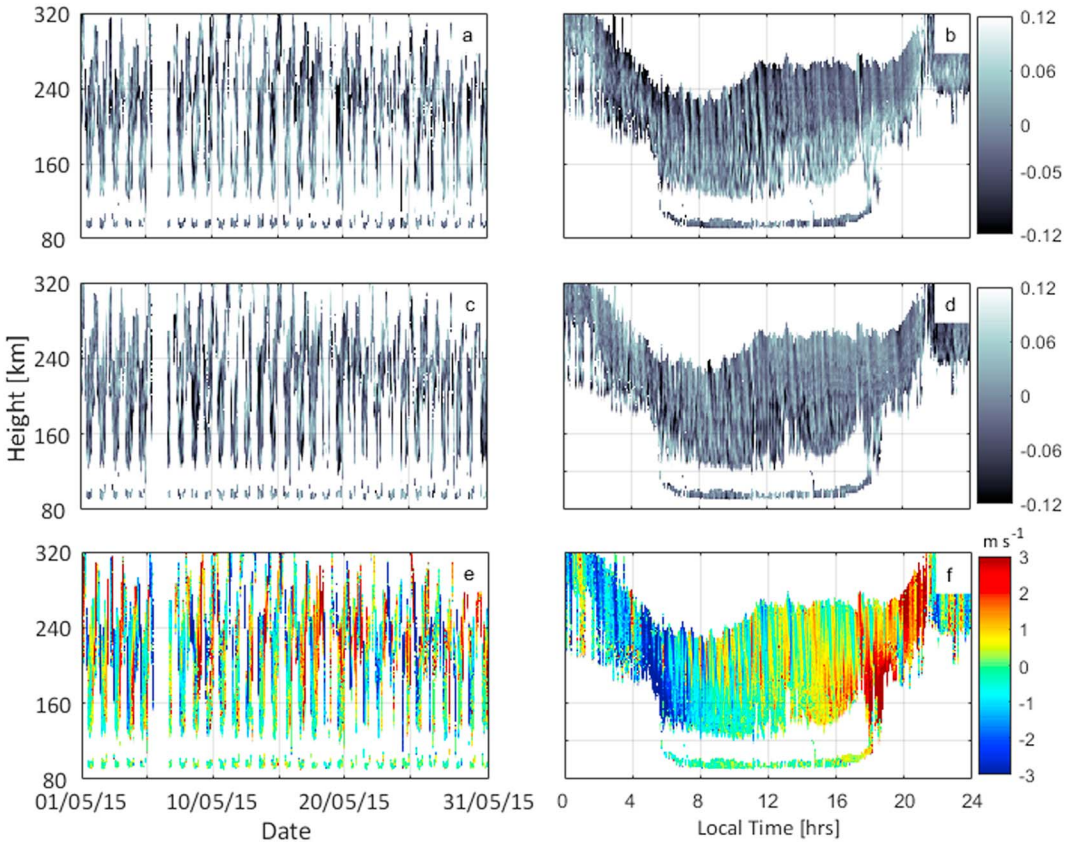

Figure 1. Data from Wallops Island, VA, Dynasonde obtained during January 2015: (a and b) zonal tilt, (c and d) meridional tilt, and (e and f) Doppler speed, for the whole month (a, c, and e), and also a subset from 25 January 2015 (b, d, and f).

The height resolution associated with the results is usually below 1 km. For our purposes, we interpolate the data to a 2-km fixed height grid. Figure 1 illustrates the intermediate data products obtained at this step. Figures 1a, 1c, and 1e show the monthlong data sets of zonal and meridional tilts and Doppler speed for the month of January 2015, highlighting features of the data sampling. Figures 1b, 1d, and 1f show a 24-hr subset of the same data on 25 January 2015, highlighting the features due to wave propagation. It is immediately obvious that TID activity is common from the slightly tilted stripes that can be observed in all three data sets. Note that this kind of visualization of the wave activity is similar to a now-standard product of Dynasonde analysis available in real time at every station.

In this study we are mainly concerned with the average wave spectrum, and not individual events. A usual assumption is made that functional dependence of the Doppler speed and electron density wave-induced perturbations is unambiguously related to the functional dependence of the tilt perturbations (Negrea et al., 2016). Given that at any specific altitude the data contain gaps, the use of traditional (fast Fourier transform-based) spectral analysis methods is not feasible. We employ a technique recently described by Negrea and Zabotin (2016), which is a combination of the Lomb-Scargle and Welch methods, with an added filtering criterion. A sliding window approach is used, with a window width of 4 hr and a 1-hr step. For each window position, an implementation of the Lomb-Scargle method is used to determine the power spectrum $P(f)$:

$$P(f) = \frac{1}{N}\left[\frac{\left(\sum_i (x_i - \bar{x})\ \cos\omega(t_i - \tau)\right)^2}{\sum_i \cos^2\omega(t_i - \tau)} + \frac{\left(\sum_i (x_i - \bar{x})\ \sin\omega(t_i - \tau)\right)^2}{\sum_i \sin^2\omega(t_i - \tau)}\right] \quad (6)$$

where $\bar{x} = \frac{1}{N}\sum_i x_i$, $\tan(2\omega\tau) = \frac{\sum_i \sin 2\omega t_i}{\sum_i \cos 2\omega t_i}$, $\omega = 2\pi f$ is the angular frequency, and N is the size of the data set

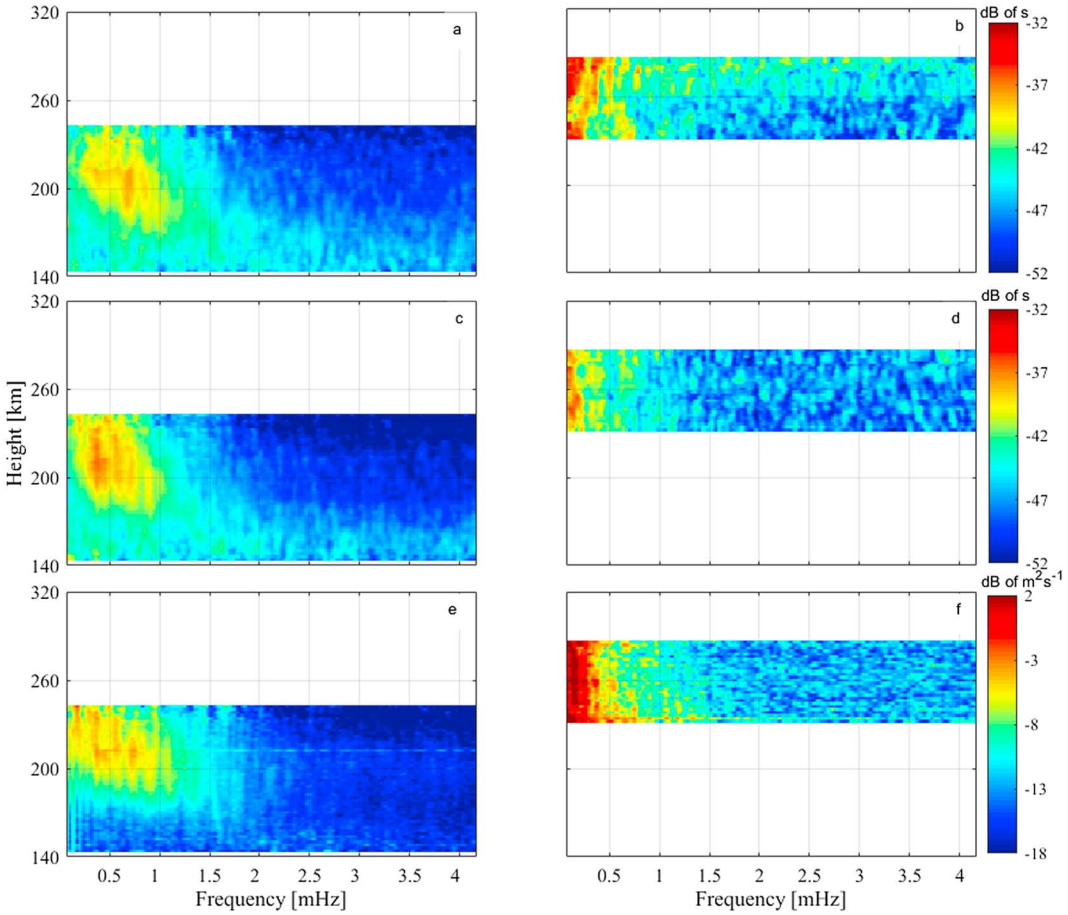

Figure 2. Height variation of the mean TID PSD for January 2015 at Wallops Island, VA, for the (a and b) zonal tilt, (c and d) meridional tilt, and (e and f) Doppler speed. The results were obtained independently for data taken during daytime (a, c, and e) and nighttime (b, d, and f).

(t_i, x_i). This approach is widely used for the spectral analysis of nonuniformly sampled data in a variety of scientific fields (Lomb, 1976; Scargle, 1982, Horne & Baliunas, 1986; Zhou et al., 1997; Schimmel, 2001; Thong et al., 2004; Hocke & Kämpfer, 2009). However, results by Munteanu et al. (2016) have shown that in the case of large data gaps, equation (2) can no longer reproduce the real power spectrum with sufficient accuracy. To account for this, a filtering criterion is used to establish the validity of results for each window position. As a direct consequence of Parseval's theorem:

$$\sum_1^{N_f} P_i \cdot (t_N - t_1) \cdot \Delta f_i + \xi = \sigma^2, \tag{7}$$

where P_i is the power calculated for frequency bin Δf_i using equation (6), N_f is the total number of frequency bins, $t_N - t_1$ is the length of the time interval considered, σ^2 is the variance in the time domain, and the extra term ξ sums up the effect due to noise and nonstationarity of the data series. In the case of a stationary spectrum with minimal or no noise, $\xi = 0$. This is rarely the case for real data, and a threshold value separating valid data from those excessively distorted may be determined for ξ. Here we will use $\xi_0 = 0.04 \cdot \sigma^2$ as the threshold value, following Negrea and Zabotin (2016). For all window positions for which $\xi \leq \xi_0$, we consider the power spectrum obtained using equation (6) to be valid. Finally, following the approach described by Welch (1967), we determine the mean PSD by averaging the results for all valid subintervals. In addition to the mean PSD, an associated standard deviation is also calculated.

To summarize, our method consists of the following steps: split a monthlong data set into 4-hr-long subintervals with a 3-hr overlap between adjacent subintervals; for each subinterval, use equation (6) to determine $P(f)$, and equation (7) to determine ξ; and finally, determine the mean PSD using only the results associated with $\xi \leq \xi_0$.

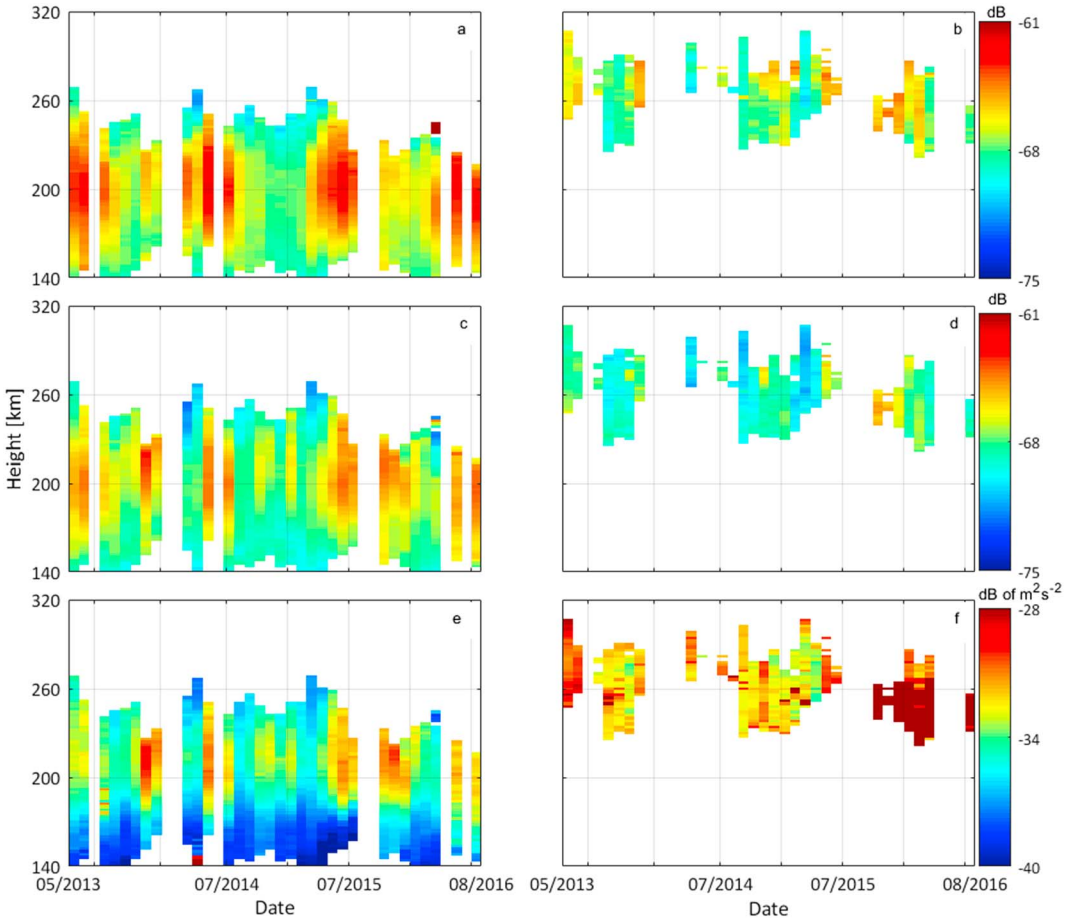

Figure 3. Variation of the height stratified, monthly averaged PSD integral between May 2013 and August 2016, at Wallops Island, VA. The different panels correspond to (a and b) the zonal tilt, (c and d) the meridional tilt, and (e and f) the Doppler speed. The positions of the vertical grid lines are chosen to correspond to the months of July and December, facilitating the observation of seasonal variability. The results were obtained independently for data taken during daytime (a, c, and e) and nighttime (b, d, and f).

3. Results

The filtering off excessively distorted data makes our method a robust spectral analysis technique, and it results an accurate estimate of the mean TID PSD representative for a given time interval. Figure 2 shows the zonal and meridional tilts and Doppler speed PSD for the data set in Figures 1a, 1c, and 1e, covering the entire month of January 2015. Due to the natural diurnal variability that is highlighted in Figure 1, results characterizing the daytime and nighttime ionosphere cover different altitude ranges: 140–260 km and 230–320 km, respectively. To avoid any confusion between the diurnal and seasonal variability, the daytime and nighttime measurements were analyzed independently for each parameter, where "daytime" is defined as the time interval between local sunrise and sunset and "nighttime" as the time interval between local sunset and sunrise. The main features are the same for all three parameters, showing a gradual shift of the dominant wave activity toward lower frequencies with the altitude, due to a combination of two factors, the decrease of the buoyancy frequency and the increase of dissipation stronger affecting short-period waves. Notice that while the minima and maxima for the tilt PSDs are different from the minimum and maximum values of the Doppler speed PSD, the range for all three is similar, approximately 20 dB. The higher noise level in the nighttime PSDs is mostly due to the smaller amount of subintervals for which $\xi \leq \xi_0$.

Figure 2 represents a "snapshot" of the mean TID PSD, valid for a single month. The dominant features of the PSD height variation do not change significantly from month to month, but the overall amplitude varies by several dB within a year. In order to observe the seasonal variability of the TID activity, we integrate the PSD over the frequency band 0.069–4.17 MHz at each altitude for each month, where the lowest accessible

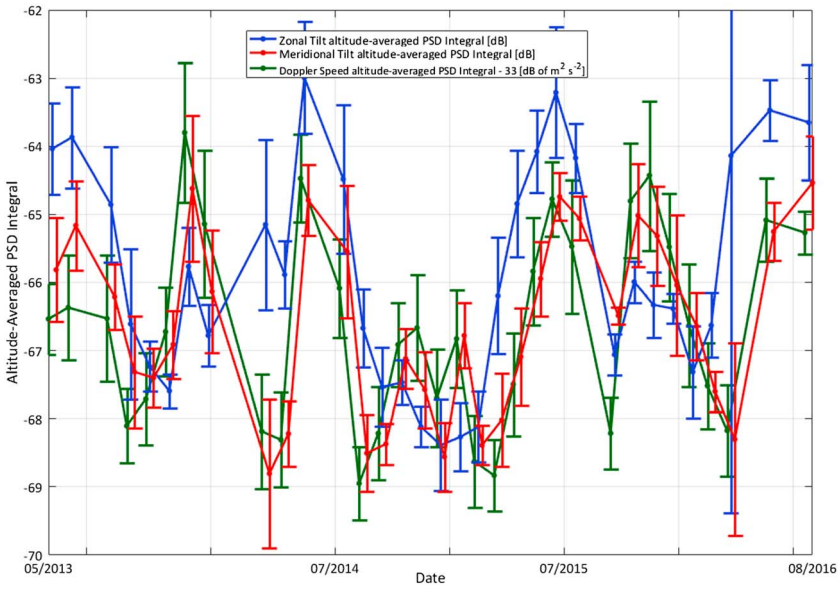

Figure 4. Altitude-averaged PSD integrals and associated standard deviations, representative for the 180–240 km altitude range during daytime. The positions of the vertical grid lines correspond to the months of July and December.

frequency is dictated by the choice in window size (4 hr), and the highest available frequency is dictated by the data sampling (2 min). The resulting PSD integral is an estimator of the ionospheric variability due to TIDs. Figure 3 shows the variation of the PSD integral over the entire 40-month period from 1 May 2013 to 31 August 2016, for the zonal and meridional tilts and the Doppler speed, where the position of the vertical grid lines is chosen to correspond to the months of July and December. Note that unlike other methods used for the study of TIDs and AGWs, the Dynasonde technique allows for height stratified spectral results to be obtained, as can be seen in Figures 2 and 3. While altitude variability is definitely present, the main observed feature is a strong semiannual variation during daytime, with periods of increased TID activity 3–4 monthlong in the summer and winter, with an increase of the PSD integral of up to 5–6 dB, mainly manifesting itself in the height interval 180–240 km. Possible explanations for the altitude range of this feature are a higher amplitude of AGWs there, or a stronger ionospheric response in the form of TIDs, or a combination of these factors. The nighttime results are inconclusive due to the high accuracy threshold of the spectral analysis technique, and, consequently, more limited amount of qualifying data available at nighttime for this particular location.

To further investigate the seasonal variability of TID activity, an altitude-averaged PSD integral is used, based on the daytime results displayed in Figures 3a, 3c, and 3e. For each month, an average value is determined over the altitude range 180–240 km. Additionally, an associated standard deviation is determined using the basic principles of error propagation: first, the standard deviation associated with each mean PSD (dependent on both frequency and height) is used to determine the standard deviation associated with the integral PSD (dependent only on height); and second, an error estimate is obtained for the average integral PSD. The result is shown in Figure 4, for the zonal and meridional tilts and the Doppler speed, where again the positions of the vertical grid lines are chosen to correspond to the months of July and December. The Doppler speed PSD depends solely on the amplitude of TID activity (equation (3)), while a change in propagation direction can also affect the tilt PSDs (equation (5)) due to the vector character of the tilt. The semiannual variability is again highlighted for the entire period, for all three parameters. This is in contrast with Frissell et al. (2016), which indicate the existence of a single annual peak in TID activity, occurring during winter. Somewhat similarly to our work, Shiokawa et al. (2003) indicated the existence of a semiannual variation in TID activity over Japan, at similar latitudes, but in that case the airglow all-sky imager limited the analysis to nighttime TIDs, while in our analysis the seasonal variation is attributed to daytime events. Another similar feature was observed by Kotake et al. (2006) over the Eastern North American continent using Global Positioning System total electron content measurements, but our work reveals a significantly larger amplitude for this semiannual variation in TID activity. The amplitude of the summer and winter peaks varies

between 2 and 6 dB, with no other clear trend, suggesting that the semiannual variation is a constant feature for the ionosphere above Wallops Island, VA. Possible causes for this are the variation of the sources of AGWs, and changes in the neutral winds, which in turn affect wave propagation and dissipation.

For both the zonal and meridional tilts, the semiannual variation is present, with two additional observations. The winter peaks are generally 1–3 dB smaller than the adjacent summer peaks, probably due to seasonal changes in the background electron density distribution. Additionally, a change can be observed in the relative amplitude of the zonal and meridional tilts, with higher amplitudes for the zonal tilt during summer, and nearly equal amplitudes during winter. Due to the directional nature of the tilts, this is indicative of a change in the propagation direction of some of the underlying AGW packets. The winter of 2014 must be mentioned as a particular case, during which we notice a significantly larger peak for the Doppler speed PSD than for the two components of the tilt. Although this does not contradict any of the assumptions made or the conclusions provided here, this feature requires further investigation.

4. Conclusions

This paper addresses the issue of seasonal variability of TIDs in the midlatitude thermosphere-ionosphere above the eastern United States. An extensive data set of ionospheric tilts and vertical Doppler speed, covering more than three years between 1 May 2013 and 31 August 2016, was obtained using the Dynasonde-capable instrument at Wallops Island, VA. The data are height stratified with a varying resolution between tens to hundreds of meters, and we interpolate to a fixed height grid with a 2 km resolution between 140 and 320 km altitude. A method of spectral analysis based on the Lomb-Scargle and Welch methods is used to mitigate the problem of data gaps and determine the mean PSD describing the ionospheric variability. This is done separately for each month, at each altitude, and independently for daytime and nighttime, resulting in 40 pairs of height-stratified PSDs, covering the frequency band 0.069–4.17 MHz (periods between 4 min and 4 hr).

While the frequency-altitude patterns remain similar throughout all the data sets, the magnitude changes by several dB within a year. The individual PSDs are integrated over frequency, and the resulting integral PSD is used to highlight a seasonal variability of daytime TIDs, likely caused by AGWs in the altitude range 180–240 km, likely composed of an annual and semiannual components. The peaks in TID activity occur during the summer and winter seasons, with an amplitude that varies between 2 and 6 dB. No clear trend could be discerned regarding the relative amplitude of the summer and winter peaks, nor was any other long-term trend observed. These conclusions are supported by the results obtained with all three parameters, with minor differences.

This paper clarifies the issue of seasonal variability of TIDs over the eastern United States, showing the existence of a semiannual variability of significant amplitude. Additional work is required to investigate the cause of this variability, but it is likely that it has an impact on the mean thermospheric flow, and on applications influenced by ionospheric perturbations, such as communication and positioning systems. Finally, the use of Dynasonde measurements from multiple locations would allow for further characterization of this variability.

Acknowledgments
This work was supported by the Office of Naval Research Basic Research Challenge program through award N000141310348. Part of this work was conducted while one of the authors (C. N.) held a University of Colorado Assistantship. Additional support was provided by a grant of the Romanian Ministry of National Education, UEFISCDI, project PN-III-P1-1.1-PD-2016-1918, and by NSF grant 1643119. Field support of Wallops Dynasonde operation has been provided, in part, by the staff of the NASA's Wallops Flight Facility. The Dynasonde data are accessible through the project's Web site (http://surf.colorado.edu) upon request to the author (N. Z.) as well as through NGDC's MIRRION server (ftp://ftp.ngdc.noaa.gov/ionosonde/data/WI937/). The authors want to thank Tim Fuller-Rowell, Oleg Godin, and Mihail Codrescu for valuable discussions regarding the connection between AGWs, TIDs, ionospheric variability, and Dynasonde data.

References

Borries, C., Jakowski, N., & Wilken, V. (2009). Storm induced large scale TIDs observed in GPS derived TEC. *Annales de Geophysique*, *27*(4), 1605–1612. https://doi.org/10.5194/angeo-27-1605-2009

Bristow, W. A., Greenwald, R. A., & Samson, J. C. (1994). Identification of high latitude acoustic gravity wave sources using the Goose Bay HF radar. *Journal of Geophysical Research*, *99*(A1), 319–331. https://doi.org/10.1029/93JA01470

Djuth, F. T., Zhang, L. D., Livneh, D. J., Seker, I., Smith, S. M., Sulzer, M. P., et al. (2010). Arecibo's thermospheric gravity waves and the case for an ocean source. *Journal of Geophysical Research*, *115*, A08305. https://doi.org/10.1029/2009JA014799

Frissell, N. A., Baker, J. B. H., Ruohoniemi, J. M., Gerrard, A. J., Miller, E. S., Marini, J. P., et al. (2014). Climatology of medium-scale traveling ionospheric disturbances observed by the midlatitude Blackstone SuperDARN radar. *Journal of Geophysical Research: Space Physics*, *119*, 7679–7697. https://doi.org/10.1002/2014JA019870

Frissell, N. A., Baker, J. B. H., Ruohoniemi, J. M., Greenwald, R. A., Gerrard, A. J., Miller, E. S., & West, M. L. (2016). Sources and characteristics of medium-scale traveling ionospheric disturbances observed by high-frequency radars in the North American sector. *Journal of Geophysical Research: Space Physics*, *121*, 3722–3739. https://doi.org/10.1002/2015JA022168

Garcia, F. J., Kelley, M. C., Makela, J. J., & Huang, C.-S. (2000). Airglow observations of mesoscale low-velocity traveling ionospheric disturbances at midlatitudes. *Journal of Geophysical Research*, *105*(A8), 18,407–18,415. https://doi.org/10.1029/1999JA000305

Grocott, A., Hosokawa, K., Ishida, T., Lester, M., Milan, S. E., Freeman, M. P., et al. (2013). Characteristics of medium-scale traveling ionospheric disturbances observed near the Antarctic Peninsula by HF radar. *Journal of Geophysical Research: Space Physics*, *118*, 5830–5841. https://doi.org/10.1002/jgra.%2050515

Hernandez-Pajares, M., Juan, J. M., & Sanz, J. (2006). Medium-scale traveling ionospheric disturbances affecting GPS measurements: Spatial and temporal analysis. *Journal of Geophysical Research*, *111*, A07S11. https://doi.org/10.1029/2005JA011474

Hocke, K., & Kämpfer, N. (2009). Gap filling and noise reduction of unevenly sampled data by means of the Lomb-Scargle periodogram. *Atmospheric Chemistry and Physics*, *9*, 4197–4206. https://doi.org/10.5194/acp-9-4197-2009

Horne, J. H., & Baliunas, S. L. (1986). A prescription for period analysis of unevenly sampled time series. *Astrophysical Journal*, *302*, 757–763. https://doi.org/10.1086/164037

Ishida, T., Hosokawa, K., Shibata, T., Suzuki, S., Nishitani, N., & Ogawa, T. (2008). SuperDARN observations of daytime MSTIDs in the auroral and mid-latitudes: Possibility of long-distance propagation. *Geophysical Research Letters*, *35*, L13102. https://doi.org/10.1029/2008GL034623

Kotake, N., Otsuka, Y., Tsugawa, T., Ogawa, T., & Saito, A. (2006). Climatological study of GPS total electron content variations caused by medium-scale traveling ionospheric disturbances. *Journal of Geophysical Research*, *111*, A04306. https://doi.org/10.1029/2005JA011418

Lomb, N. R. (1976). Least-squares frequency analysis of unequally spaced data. *Astrophysics and Space Science*, *39*, 447–462. https://doi.org/10.1007/BF00648343

Munteanu, C., Negrea, C., Echim, M., & Mursula, K. (2016). Effect of data gaps: Comparison of different spectral analysis methods. *Annales de Geophysique*, *34*(4), 437–449. https://doi.org/10.5194/angeo-34-437-2016

Negrea, C., Zabotin, N., Bullett, T., Codrescu, M., & Fuller-Rowell, T. (2016). Ionospheric response to tidal waves measured by Dynasonde techniques. *Journal of Geophysical Research: Space Physics*, *121*, 602–611. https://doi.org/10.1002/2015JA021574

Negrea, C., Zabotin, N., Bullett, T., Fuller-Rowell, T., Fang, T.-W., & Codrescu, M. (2016). Characteristics of acoustic gravity waves obtained from Dynasonde data. *Journal of Geophysical Research: Space Physics*, *121*, 3665–3680. https://doi.org/10.1002/2016JA022495

Negrea, C., & Zabotin, N. A. (2016). Mean spectral characteristics of acoustic gravity waves in the thermosphere-ionosphere determined from Dynasonde data. *Radio Science*, *51*, 213–222. https://doi.org/10.1002/2015RS005823

Oliver, W. L., Fukao, S., Yamamoto, Y., Takami, T., Yamanaka, M. D., Yamamoto, M., et al. (1994). Middle and upper atmosphere radar observations of ionospheric density gradients produced by gravity wave packets. *Journal of Geophysical Research*, *99*(A4), 6321–6329. https://doi.org/10.1029/94JA00171

Otsuka, Y., Shiokawa, K., Ogawa, T., & Wilkinson, P. (2004). Geomagnetic conjugate observations of medium-scale traveling ionospheric disturbances at midlatitude using all-sky airglow imagers. *Geophysical Research Letters*, *31*, L15803. https://doi.org/10.1029/2004GL020262

Otsuka, Y., Suzuki, K., Nakagawa, S., Nishioka, M., Shiokawa, K., & Tsugawa, T. (2013). GPS observations of medium-scale traveling ionospheric disturbances over Europe. *Annales de Geophysique*, *31*(2), 163–172. https://doi.org/10.5194/angeo-31-163-2013

Paul, A. K., Wright, J. W., & Fedor, L. S. (1974). The interpretation of ionospheric radio drift measurements-VI. Angle-of-arrival and group path [echolocation] measurements from digitized ionospheric soundings: The group-path vector. *Journal of Atmospheric and Terrestrial Physics*, *36*, 193,214. https://doi.org/10.1016/0021-9169(74)90040-3

Scargle, J. D. (1982). Studies in astronomical time series analysis. II. Statistical aspects of spectral analysis of unevenly spaced data. *Astrophysical Journal*, *263*, 835–853. https://doi.org/10.1086/160554

Schimmel, M. (2001). Emphasizing difficulties in the detection of rhythms with Lomb-Scargle periodograms. *Biological Rhythm Research*, *32*(3), 341–346. https://doi.org/10.1076/brhm.32.3.341.1340

Sedgemore, K. J. F., Williams, P. J. S., Jones, G. O. L., & Wright, J. W. (1996). A comparison of EISCAT and Dynasonde measurements of the auroral ionosphere. *Annales Geophysicae*, *14*(12), 1403–1412. https://doi.org/10.1007/s005850050401

Shiokawa, K., Ihara, C., Otsuka, Y., & Ogawa, T. (2003). Statistical study of nighttime medium-scale traveling ionospheric disturbances using midlatitude airglow images. *Journal of Geophysical Research*, *108*(A1), 1052. https://doi.org/10.1029/2002JA009491

Thong, T., McNames, J., Aboy, M., & Oken, B. (2004). Averaged Lomb periodograms for non-uniform sampling. *Conference of the IEEE Engineering in Medicine and Biology Society*, *1*, 271–274.

Welch, P. D. (1967). The use of fast Fourier transform for the estimation of power spectra: A method based on time averaging over short, modified periodograms. *IEEE Transactions on Audio and Electroacoustics*, *15*(2), 70–73. https://doi.org/10.1109/TAU.1967.1161901

Wright, J. W., & Pitteway, M. L. V. (1979). Real-time data acquisition and interpretation capabilities of the Dynasonde. 1. Data acquisition and real-time display. *Radio Science*, *14*(5), 815–825. https://doi.org/10.1029/RS014i005p00815

Wright, J. W., & Pitteway, M. L. V. (1999). A new data acquisition concept for digital ionosondes: Phase-based echo recognition and real-time parameter estimation. *Radio Science*, *34*(4), 871–882. https://doi.org/10.1029/1999RS900039

Zabotin, N. A., Godin, O. A., & Bullett, T. W. (2016). Oceans are a major source of waves in the thermosphere. *Journal of Geophysical Research: Space Physics*, *121*, 3452–3463. https://doi.org/10.1002/2016JA022357

Zabotin, N. A., Wright, J. W., & Zhbankov, G. A. (2006). NeXtYZ: Three-dimensional electron density inversion for Dynasonde ionograms. *Radio Science*, *41*, RS6S32. https://doi.org/10.1029/2005RS003352

Zhou, Q. H., Sulzer, M. P., & Tepley, C. A. (1997). An analysis of tidal and planetary waves in the neutral winds and temperature observed at low-latitude E region heights. *Journal of Geophysical Research*, *102*, 11,491–11,505. https://doi.org/10.1029/97JA00440